A FULLY TRANSIENT ROD PUMP MODEL WITH HYDRAULIC DAMPING

Walter B. Fair, Jr.
The University of Texas at Austin

ABSTRACT

Mathematical rod pump models are used in the design and optimization of lift systems. Most models are based on the damped wave equation, assuming steady state cyclic behavior and empirical damping factors. Such models cannot be used for fully transient analyses.

This paper extends the rod pump model based on fluid flow in the reservoir, wellbore and tubing. Rod drag is determined from multiphase flow modeling using the full momentum, mass and energy balance equations with friction loss terms based on standard pipe flow correlations. The effect of transient reservoir flow is incorporated by a radial flow reservoir model for inflow to the wellbore.

Development of the model is discussed and shown to predict complex system behavior. The model is then used to evaluate damping factors and suggest the potential for additional surveillance methods based on transient fluid and rod behavior.

INTRODUCTION

Rod pumps are normally modeled using the damped wave equation. A history and literature review of rod pump modeling has previously been presented by several authors (cf. Lekia and Evans (1995)). Most of the recent models can be traced back to Gibbs (1963) work where a numerical solution to the damped wave equation was presented. Unfortunately the application of the Gibbs formulation requires estimation of the damping factor which may be difficult. In fact some authors suggest that different damping factors should be used on the upstroke and downstroke calculations, but this leads to questions as to what portion of the rod string is most important, since portions of the string do not necessarily travel uniformly in the same direction at the same time.

Furthermore, most rod pump models assume constant tubing pressure and either ignore reservoir flow or invoke steady state flow from the reservoir as boundary conditions. However, observation of the tubing pressure gauge on a pumping well can attest that the tubing pressure is not necessarily constant. It is also obvious from a consideration of the rod pump operation that fluid flow is not steady state, but at least varies cyclically depending on the rod motion and valve operations.

As a result of these considerations, a more complex rod pump modeling system has been developed that removes the empirical damping factor from the rod drag calculations, couples fluid friction and rod drag forces, represents transient flow throughout the system, and couples the rod pump model to a transient flow reservoir model. This system allows the evaluation of the various effects so that it can be determined when it is valid to ignore them and also allows the evaluation of new analysis procedures that make use of the transient system behavior.

Since the measurement of transient surface pressures is extremely simple, the potential application to surveillance of marginal wells appears to be obvious, however, methods for evaluation of transient surface pressures are needed. In that regard, the model developed in this work presents an initial step toward improved surveillance methods using easily measured surface pressure data.

MATHEMATICAL MODEL

The flow system defined in this work is based on an abstract directed acyclic graph as discussed by Aho et al. (1983) where each equipment item is represented by a node and arcs represent the flow streams or connections between equipment. This is a standard approach previously described by various authors to represent flow networks. cf. Daugherty and Franzini (1965); Himmelblau and Bischoff (1968). Using an object oriented software design philosophy, equipment objects (nodes) are those items with volume and state changes occurring internally, while flow streams (arcs) have no volume and serve mainly as pressure measurement points and connections between items. As such, the equipment items contain internal calculations to determine their state and performance, while streams consist only of flow stream parameters.

For each equipment object within the network, the conservation of mass, the conservation of linear momentum and the conservation of energy can be applied to represent fluid flow and mass storage within the equipment that the node represents. Examples are pipes, wells, separators, tanks, headers, etc.
Flow streams, however, have no volume and represent the connections between equipment nodes. It is assumed that streams have properties of mass flow rates, temperature and pressure, but no internal mass is stored within a flow stream. The continuity of flowing properties through the flow streams is assumed and the streams represent connections between items in the flow network.

The overall network is represented computationally as an object containing fluid property relations, a list of flow equipment items and a list of flow streams. Each equipment item is identified by an equipment type and a name, while flow streams are only identified by the equipment items that they connect.

The fundamental equations describing flow in the network (cf. Daugherty (1965)) consist of mass, momentum, and energy balance relations for each subpart of the network along with continuity relationships. Since we will implement the network using detailed physical models for each equipment node, all of the balances will automatically be satisfied over every part of the network and the network as a whole. In addition a continuity constraint is needed, which is automatically satisfied by detailed internal modeling within each node and the constraint that each stream (i.e. connection between nodes) can have only a single temperature, pressure, and flow rate at any time. In other words, the outlet conditions from one equipment item must be the same as the inlet conditions for the following item. As will be seen, due to the implementation, this will be automatically ensured in the flow network model.

In order to solve the fundamental flow equations in the flow network, an iterative multi-pass algorithm has been developed. While considering flow especially through junctions where mass conservation requires a balance between the flow rates, pressures and temperatures of individual complex flow equipment items, it is apparent that the simultaneous solution of the equations of momentum, mass, and energy throughout a complex network would be difficult and likely impractical to implement. As a result, an iterated sequential solution algorithm has been devised and the following solution procedure has been implemented.

1) Sort the network equipment items in order from sources to sinks using the following procedure:
    a) Create an empty list of equipment items, then search through the network equipment and add all equipment items that do not have a defined inlet.
    b) For each equipment item in the list
        i) For each outlet stream, find the equipment associated with the outlet and add it to the list.
2) Set simulation time to zero and initialize the flow system using the following procedure:
    a) Beginning at the sources, traverse the flow network and set all rates to zero and all temperatures to a specified ambient temperature with appropriate fluid contents.
    b) Beginning at the sinks, traverse the network in a reverse direction and compute the inlet pressure for each equipment item considering static equilibrium within each equipment item.

3) Iterate through the network flow calculations until the flow rates, temperature and pressure of all flow streams do not change within a specified tolerance using the following procedure:
   a) Determine the flow rates at the sources of the network based on control considerations.
   b) Beginning at the sources, traverse the flow network in a forward direction and solve the applicable flow equations to determine the outlet flow rates for each equipment item in order assuming that the pressure, temperature and inlet flow rates are known.
   c) Beginning at the sinks, traverse the flow network in a reverse direction to compute the pressure at the inlet of each flow equipment item assuming that the flow rates, temperature and outlet pressures are known.
   d) Beginning at the sources, traverse the network in a forward direction and compute the outlet temperature for each equipment item assuming the flow rates, pressures and inlet temperature are known.
   e) If pressure, flow rate or temperature changes during the iteration exceed specified thresholds, repeat the iteration from 3b.
   f)
4) Print or save necessary information, advance the time step and return to step 3.

Even though the flow network is general and capable of representing a wide variety of complex field configurations, only the items related directly to a beam pumping well are presented here. The principle equipment items considered in this paper are completions, casing, pumps, tubing, rod strings, and flowlines. Constant outlet pressure is assumed in all models presented here. Besides the fundamental physical laws governing fluid flow through the various equipment items, a black-oil fluid model is used in this study, with liquid and vapor hydrocarbon phases and an aqueous phase.

Pipe flow equations. A significant portion of an oil field facility consists of fluid flow in pipes. In the rod pump model described here we specifically are interested in flow in the tubing and rod annulus as well as flow in the surface flowline. As a result we must solve the fundamental equations for fluid flow consisting of the mass balance, momentum balance and energy balance relations. In this model we follow the general momentum and mass balance formulation detailed in the RELAP5 (2012) documentation and use a total energy balance for thermal effects. This same approach has been used by other authors to represent fluid flow in wellbores; cf. Shirdel (2010).

For modeling purposes, the fluid system is represented by 2 phases: liquid and gas. The liquid consists of both hydrocarbon liquid (oil) and water and for modeling purposes oil and water are assumed to move at the same velocity (i.e. no slip condition). In addition, the difference in pressure between the phases is ignored, so that the system can be represented by a single value of pressure at each point in the pipe. For many systems this assumption appears to be reasonable, but for flow of very viscous oil, the assumption should be reviewed and a full three phase system should be used to represent fluid flow. Radial variations inside the pipe are also ignored, so that the flow is represented as one dimensional with variations accounted for by friction factors for each phase as well as slip between phases. In contrast to the RELAP5 formulation, annular flow is also considered here, so that the same equations can be used for flow in the tubing and rod annulus as well as in piping.

Flow of fluids in pipes is represented by momentum balance equations for the liquid and gas phases, mass balance equations for the total mass, the liquid mass and the water mass, and total energy balance equation. The use of these 6 relations allows the determination of liquid and gas velocity, pressure, liquid holdup (i.e. liquid volume fraction), water cut, and temperature. Note that the momentum relations are simplified by expanding the partial derivative of momentum and substituting the mass balance relationship. The 6 relations are shown in the following equations.

$$H_L\rho_L\frac{\partial v_L}{\partial t} + H_L\rho_L v_L\frac{\partial v_L}{\partial x} + 144g_c\frac{\partial}{\partial x}(H_L p) + H_L\rho_L g\sin\theta + (F_{wL} + F_{aL}) - F_{GL} = 0 \quad \text{.....(1}$$

$$H_G\rho_G\frac{\partial v_G}{\partial t} + H_G\rho_G v_G\frac{\partial v_G}{\partial x} + 144g_c\frac{\partial}{\partial x}(H_G p) + H_G\rho_G g\sin\theta + (F_{wG} + F_{aG}) + F_{GL} = 0 \quad \text{.....(2}$$

$$\frac{\partial}{\partial t}(H_L\rho_L + H_G\rho_G) + \frac{\partial}{\partial x}(H_L\rho_L v_L + H_G\rho_G v_G) = 0 \quad \text{.....(3}$$

$$\frac{\partial}{\partial t}(H_L\rho_L) + \frac{\partial}{\partial x}(H_L\rho_L v_L) = 0 \quad \text{.....(4}$$

$$\frac{\partial}{\partial t}(H_L[1-f_w]\rho_o) + \frac{\partial}{\partial x}(H_L[1-f_w]\rho_o v_L) = 0 \quad \text{.....(5}$$

$$\begin{aligned}\frac{\partial}{\partial t}\left[H_L\rho_L\left(h_L + \frac{{v_L}^2}{2g_cJ_c} - \frac{144p}{J_c\rho_L}\right) + H_G\rho_G\left(h_G + \frac{{v_G}^2}{2g_cJ_c} - \frac{144p}{J_c\rho_G}\right)\right] + (H_L\rho_L v_L + H_G\rho_G v_G)g\sin\theta \\ + \frac{\partial}{\partial x}\left[H_L\rho_L v_L\left(h_L + \frac{{v_L}^2}{2g_cJ_c}\right) + H_G\rho_G v_G\left(h_G + \frac{{v_G}^2}{2g_cJ_c}\right)\right] + \frac{S}{A}U(T - T_{ext}) = 0\end{aligned} \quad \text{.....(6}$$

In order to use the momentum balance equations, it is necessary to determine the drag force per unit volume terms, F_{wL}, F_{wG}, F_{aL}, F_{aG}, and F_{LG}, representing the drag force of the pipe wall on the liquid phase, the drag force of the pipe wall on the gas phase, the drag force of the annulus wall on the liquid phase, the drag force of the annulus wall on the gas phase and the interfacial drag force of the liquid phase on the gas phase, respectively. It is apparent that these terms depend on the relative velocities, the volume fraction of each phase, the surface area of contact between pipe and phases, and also the flow pattern. Details of flow pattern determination and the form of the drag terms can be found in Shoham (2006) and Govier and Aziz (2008), as well as the form used in this work and documented in the RELAP5 (2012) documentation. Figures 1 and 2 show schematic views of the flow regimes for two phase flow used in this work.

It is assumed that the wall friction is adequately described by the friction factors determined as described in the RELAP5 documentation. For annular flow, an additional friction term is needed to describe the drag on the annulus. By considering a force balance on an infinitely thin surface at the annulus diameter, it is apparent that when the same flow velocity is used in an equivalent virtual fluid computation on the inside of the annulus, the force balance constraint indicates that the drag forces on the wall of the inside flow must balance the drag forces on the annulus. Since the major use of annular flow in this work is to describe flow in the tubing and rod annulus, the internal flow velocity is assumed to be the difference between the fluid velocity and the rod velocity.

At each time step the flow pattern is found and the corresponding drag forces are computed using the velocity and volume fractions at the previous time step. While this procedure is general, it should be noted that in the present study bubble flow was nearly always found for vertical (i.e. wellbore) flow and a stratified flow for horizontal pipe flow. In addition, the annular drag terms are assumed to be zero for pipe flow, but for flow in the tubing and rod annulus drag terms are computed from other friction factor correlations as described.

The pipe flow equations are solved in 3 steps as described in the network solution algorithm. Each of the equations is converted to finite difference form using a forward time difference. Since the resulting difference equations are nonlinear, a Newton iteration procedure is used to search for the root of the various balance equations by defining a Jacobian matrix for each relation. The finite difference formulations are shown here. Details of the implicit solution procedure can be found in Shirdel (2010) and other references on the numerical solution of nonlinear partial differential equations.

To solve momentum equations for liquid and gas velocities assuming pressure, temperature and inlet velocity are known:

$$\begin{aligned}f_{Li}^n = {} & [(H_{Li}^n + H_{Li+1}^n)(\rho_{Li}^n + \rho_{Li+1}^n)v_{Li}^n - (H_{Li}^{n-1} + H_{Li+1}^{n-1})(\rho_{Li}^{n-1} + \rho_{Li+1}^{n-1})v_{Li}^{n-1}]\frac{\Delta x}{4\Delta t} \\ & + [H_{Li+1}^n\rho_{Li+1}^n(v_{Li}^n + v_{Li+1}^n)^2 - H_{Li}^n\rho_{Li}^n(v_{Li-1}^n + v_{Li}^n)^2] \\ & + 144g_c\left[\left(H_{Li+1}^nP_{i+1}^n + H_{Li+1}^n\rho_{Li+1}^n\sin\theta\frac{\Delta x}{144}\right) - H_{Li}^nP_i^n\right] + (F_{wL} + F_{aL} - F_{LG})\Delta x = 0\end{aligned} \quad \text{.....(7}$$

$$\begin{aligned}f_{Gi}^n = {} & [(H_{Gi}^n + H_{Gi+1}^n)(\rho_{Gi}^n + \rho_{Gi+1}^n)v_{Gi}^n - (H_{Gi}^{n-1} + H_{Gi+1}^{n-1})(\rho_{Gi}^{n-1} + \rho_{Gi+1}^{n-1})v_{Gi}^{n-1}]\frac{\Delta x}{4\Delta t} \\ & + [H_{Gi+1}^n\rho_{Gi+1}^n(v_{Gi}^n + v_{Gi+1}^n)^2 - H_{Gi}^n\rho_{Gi}^n(v_{Gi-1}^n + v_{Gi}^n)^2] \\ & + 144g_c\left[\left(H_{Gi+1}^nP_{i+1}^n + H_{Gi+1}^n\rho_{Gi+1}^n\sin\theta\frac{\Delta x}{144}\right) - H_{Gi}^nP_i^n\right] + (F_{wG} + F_{aG} + F_{LG})\Delta x = 0\end{aligned} \quad \text{.....(8}$$

To solve the mass balance equations for pressure, liquid holdup and water cut, assuming phase velocities and temperature are known, the following total, liquid and oil mass balance relations are used:

$$g_{Ti} = [(H_{Li}^n \rho_{Li}^n + H_{Gi}^n \rho_{Gi}^n) - (H_{Li}^{n-1} \rho_{Li}^{n-1} + H_{Gi}^{n-1} \rho_{Gi}^{n-1})] \frac{\Delta x}{\Delta t} + [(H_{Li}^n \rho_{Li}^n v_{Li}^n + H_{Gi}^n \rho_{Gi}^n v_{Gi}^n) - (H_{Li-1}^n \rho_{Li-1}^n v_{Li-1}^n + H_{Gi-1}^n \rho_{Gi-1}^n v_{Gi-1}^n)] = 0 \quad \text{.....(9}$$

$$g_{Li} = [H_{Li}^n \rho_{Li}^n - H_{Li}^{n-1} \rho_{Li}^{n-1}] \frac{\Delta x}{\Delta t} + [H_{Li}^n \rho_{Li}^n v_{Li}^n - H_{Li-1}^n \rho_{Li-1}^n v_{Li-1}^n] = 0 \quad \text{.....(10}$$

$$g_{oi} = [H_{Li}^n (1 - f_{wi}^n) \rho_{oi}^n - H_{Li}^{n-1} (1 - f_{wi}^{n-1}) \rho_{oi}^{n-1}] \frac{\Delta x}{\Delta t} + [H_{Li}^n (1 - f_{wi}^n) \rho_{oi}^n v_{Li}^n - H_{Li-1}^n (1 - f_{wi-1}^n) \rho_{oi-1}^n v_{Li-1}^n] = 0 \quad \text{.....(11}$$

To solve energy equation for temperature, assuming phase velocities, pressure, liquid holdup and water cut are known:

$$\begin{aligned} h_{Ti}^n = {} & \left[H_{Li}^n \rho_{Li}^n \left(h_{Li}^n + \frac{{v_{Li}^n}^2}{2 g_c J_c} - \frac{144 P_i^n}{J_c \rho_{Li}^n} \right) + H_{Gi}^n \rho_{Gi}^n \left(h_{Gi}^n + \frac{{v_{Gi}^n}^2}{2 g_c J_c} - \frac{144 P_i^n}{J_c \rho_{Gi}^n} \right) \right] \frac{\Delta x}{\Delta t} \\ & - \left[H_{Li}^{n-1} \rho_{Li}^{n-1} \left(h_{Li}^{n-1} + \frac{{v_{Li}^{n-1}}^2}{2 g_c J_c} - \frac{144 P_i^{n-1}}{J_c \rho_{Li}^{n-1}} \right) + H_{Gi}^{n-1} \rho_{Gi}^{n-1} \left(h_{Gi}^{n-1} + \frac{{v_{Gi}^{n-1}}^2}{2 g_c J_c} - \frac{144 P_i^{n-1}}{J_c \rho_{Gi}^{n-1}} \right) \right] \frac{\Delta x}{\Delta t} \\ & + \left[H_{Li}^n \rho_{Li}^n \left(h_{Li}^n + \frac{{v_{Li}^n}^2}{2 g_c J_c} \right) v_{Li}^n + H_{Gi}^n \rho_{Gi}^n \left(h_{Gi}^n + \frac{{v_{Gi}^n}^2}{2 g_c J_c} \right) v_{Gi}^n \right] \\ & - \left[H_{Li-1}^n \rho_{Li-1}^n \left(h_{Li-1}^n + \frac{{v_{Li-1}^n}^2}{2 g_c J_c} \right) v_{Li-1}^n + H_{Gi-1}^n \rho_{Gi-1}^n \left(h_{Gi-1}^n + \frac{{v_{Gi-1}^n}^2}{2 g_c J_c} \right) v_{Gi-1}^n \right] \\ & + US(T_i^n - T_{exi}^n) = 0 \end{aligned} \quad \text{.....(12}$$

To solve the flow equations, boundary conditions are also needed. For pipe flow, the required boundary conditions are obtained by specifying the inlet mass flow rates, inlet temperature and the outlet pressure at each time step. In the current model the boundary conditions are determined by the inflow and outflow relations of other equipment in the network. Of course, for fully transient flow, both inlet and outlet conditions are expected to change with time. The variations are handled by the sequentially implicit, iterative solution procedure described previously for solution of the network flow equations.

Rod string model. The rod string is modeled using a force balance that yields a form of the wave equation as presented by de Almeida Barreto Filho (2001). In this model, forces on a segment of the rod string are balanced against the stress-strain relation of the rod material and the friction drag of the fluid on the rods are considered, but Coulomb friction of the rods and tubing is ignored. For vertical wells, the Coulomb friction is probably small, but for deviated wells an additional drag force representing Coulomb friction should probably be included. The resulting equation, without Coulomb friction, describing the rod motion is shown in equation 13.

$$\frac{\partial^2 u}{\partial t^2} = \frac{E_r}{\rho_r} \frac{\partial^2 u}{\partial x^2} + g - (F_{aL} + F_{aG}) + \frac{P}{\rho_r A_r} \frac{dA_r}{dx} \quad \text{.....(13}$$

Gibbs (1963) used an empirical damping factor to account for drag forces, whereby the drag force is proportional to the rod velocity. In this work we use a friction factor formulation for flow in pipes to couple the fluid friction to the drag forces on the rods, thus the rod drag forces per unit length are described by the F_{aL} and F_{aG} terms in the pipe flow momentum equations describing flow in the tubing and rod annulus. This approach ensures consistency in the pressure drop due to flow with the corresponding rod drag forces and has previously been presented by Lekia (1995) for single phase and multiphase flow and by de Almeida Barreto Filho (2001) for single phase laminar flow.

At first thought, it would appear that the normal pipe friction terms could be used to describe drag on the rods in the tubing rod annulus. However, it is important to note that the pipe friction relations based on Reynolds number and roughness also assume uniform flow along the length of the pipe, but in the rod tubing annulus the flow is not uniform due to restrictions caused by the rod couplings. Friction factors for flow in the rod-tubing and coupling-tubing annulus were presented by Valeev. and Repin (1976) and used by both Lekia (1995) and by de Almeida

Barreto Filho (2001) in their models. In this work we also use the Valeev and Repin friction factors and apply them in a manner equivalent to that of Barreto, whereby the tubing and rod friction loss is modified by a factor depending on the additional losses imposed by the rod couplings. The follow show the relations used for liquid flow and the analogous relation used for gas.

$$F'_{aL} = F_{aL} D_t \left[1 + \frac{52000\left(\frac{D_c}{D_t} - 0.381\right)^{2.57} \left\{ 2.77 \pm 1.69 \frac{R'_{eL}}{R_{eL}} \right\}}{\frac{96}{R_{eL}} \left[1 \pm \frac{R'_e}{R_e} \left(0.2 + 0.39 \frac{D_r}{D_t} \right) \right]} \right] \quad \text{(14}$$

$$R_{eL} = \frac{\rho_L v_L (D_t - D_r)}{\mu_L}, \; R'_{eL} = \frac{\rho_L v_r (D_t - D_r)}{\mu_L} \quad \text{(15}$$

$$F'_{aG} = F_{aG} D_t \left[1 + \frac{52000\left(\frac{D_c}{D_t} - 0.381\right)^{2.57} \left\{ 2.77 \pm 1.69 \frac{R'_{eG}}{R_{eG}} \right\}}{\frac{96}{R_{eG}} \left[1 \pm \frac{R'_{eG}}{R_{eG}} \left(0.2 + 0.39 \frac{D_r}{D_t} \right) \right]} \right] \quad \text{(16}$$

$$R_{eG} = \frac{\rho_G v_G (D_t - D_r)}{\mu_G}, \; R'_{eG} = \frac{\rho_G v_r (D_t - D_r)}{\mu_G} \quad \text{(17}$$

Given the fundamental rod motion equation, the equation is converted to finite difference form for numerical solution. The methods used by Gibbs (1963) and by Everitt and Jennings (1992) are modified in this work to derive an explicit rod motion calculation whereby the time step is not assumed to be constant. Since two time levels are required to approximate the second derivative with respect to time, this allows automatic time step adjustments while the model is running. The resulting explicit finite difference equation is as follows.

$$\begin{aligned} u_i^{n+1} = [&(A_{ri+1} u_{i+1}^n - 2A_{ri} u_i^n + A_{ri-1} u_{i-1}^n) \frac{a^2 \Delta t_n (\Delta t_n + \Delta t_{n-1})}{2\Delta x^2} \\ &+ \frac{(\Delta t_n + \Delta t_{n-1})}{\Delta t_{n-1}} A_{ri} u_i^n - \frac{\Delta t_n}{\Delta t_{n-1}} A_{ri} u_i^{n-1} \\ &- \frac{A_t}{\rho_r g_c A_{ri}} (F_{aLi} + F_{aGi}) \frac{\Delta t_n (\Delta t_n + \Delta t_{n-1})}{2}] / A_{ri} \end{aligned} \quad \text{(18}$$

Initial and boundary conditions are also required for solution of the rod string motion. The initial condition is computed by assuming the rods are hanging in static equilibrium, with the stress and the corresponding strain computed from the buoyant rod weight at each point in the rod string. The boundary conditions consist of the polish rod position at each time step, u[0,t], as well as the load at the pump computed from the tubing flow and downhole pump pressure relations described below.

Surface pumping unit. In this study the Gray (1963) pumping unit model is used whereby the motion is represented by a 4 bar problem. Standard API unit dimensions are used throughout and a constant angular velocity is assumed. Future work should incorporate motor slippage, but that is not considered here. Using API pumping unit geometry nomenclature, the relations are as follows.

$$L_2 = \sqrt{(H - G)^2 + I^2} \quad \text{(19}$$

$$C_1 = \cos(\theta + \theta_c) \quad \text{(20}$$

$$C_2 = \sqrt{1 + \left(\frac{R}{L_2}\right)^2 + 2C_1 \frac{R}{L_2}} \quad \text{(21}$$

$$C_3 = \frac{1}{C_2} \left(a_a + \frac{R C_1}{C} \right) \quad \text{(22}$$

$$C_4 = \frac{R \sin(\theta + \theta_c)}{C_2 L_2} \quad \text{(23}$$

$$a_a = \frac{R^2 + L_2^2 + C^2 - P^2}{2 L_2 C} \quad \text{(24}$$

$$\alpha = \tan^{-1}\left(\frac{C_4}{\sqrt{1-C_4^2}}\right) \quad (25$$

$$\beta = \cos^{-1}(C_3) \quad (26$$

$$x_0 = \frac{1}{12}[A(\alpha+\beta) - x_{min}] \quad (27$$

$$\theta^n = \theta^{n-1} + \frac{2\pi\Delta t_n}{60/SPM} \quad (28$$

The surface polish rod position is advanced by assuming a constant angular velocity whereby 2π radians are traversed during each stroke. The surface position, shown as x_0 in Equation 27 is the surface position of the rod string at the new time step, $u[0,t_n]$.

Downhole pump. The downhole pump is modeled using a simple mass balance to determine pump pressure. Variation of pressure with position inside the pump and plunger inertia are not considered and complete separation of gas before entry into the pump is assumed in the models presented here. The internal pump volume depends on the plunger position which is equal to the bottom of the rod string. Since the fluid properties depend on pressure, the pump pressure is determined by searching for the root of Equation 29.

$$V_p^n = V_p^{n-1} + (u_L^n - u_L^{n-1}) = V_o^n B_o + V_w^n B_w + \left(V_g^n - R_s V_o^n\right) \quad (29$$

Once the internal pump pressure is known, the load on the plunger can be computed by the pressure difference between the tubing pressure above the pump and the internal pump pressure, multiplied by the net plunger area. This serves as a load boundary condition on the bottom of the rod string, whose equation of motion was previously described.

$$\frac{\partial u_L^n}{\partial x} = \frac{A_p(p_{tN}^n - p_p^n)}{E_r A_p} \quad (30$$

In addition, the pump plunger motion provides a boundary condition for mass flow into the bottom of the tubing. During the upstroke the plunger is moving upward and the volumetric flow into the bottom of the tubing is equal to the area of the pump-rod annulus times the plunger velocity and the volumetric flow into the pump from the wellbore is equal to the plunger area times the plunger velocity. Similarly, during the down stroke, the rods displace fluids inside the pump barrel, so the volumetric flow into the base of the tubing is equal to the rod area times the plunger velocity. During the stroke, the traveling and standing valves states (open or closed) are determined based on the pressure difference between the internal pump and the tubing pressure or the external wellbore pressure.

When the traveling valve is open, it is assumed that free gas inside the pump will enter the tubing and liquids will enter only when all of the free gas has been depleted from the pump. It is important to note that in all of the cases presented in this paper, no free gas in the pump is allowed since perfect separation is assumed before fluid entry into the pump.

$$q_{ot}^n = \begin{cases} (1-f_w)\frac{dV_p}{dt}B_o & \left(V_g^n - R_s V_o^n\right) \le 0 \\ 0 & \left(V_g^n - R_s V_o^n\right) > 0 \end{cases} \quad (31$$

$$q_{wt}^n = \begin{cases} f_w \frac{dV_p}{dt}B_w & \left(V_g^n - R_s V_o^n\right) \le 0 \\ 0 & \left(V_g^n - R_s V_o^n\right) > 0 \end{cases} \quad (32$$

$$q_{gt}^n = \begin{cases} \frac{dV_p}{dt}B_g & \left(V_g^n - R_s V_o^n\right) > 0 \\ 0 & \left(V_g^n - R_s V_o^n\right) \le 0 \end{cases} \quad (33$$

Reservoir and completion model. To represent transient fluid flow from the reservoir into the wellbore a radial flow reservoir model similar to that used in pressure transient analysis is used as presented by Earlougher (1977) among others. The reservoir model includes skin at the wellbore and relates the fluid flow into the well to the pressure distribution in the near well area. In contrast to normal pressure transient testing, a pressure boundary condition is applied at the wellbore, whereby the flow into the well is controlled by the pressure inside the wellbore. Since the pressure varies with pump action and annular fluid level, a constant or steady state flow rate will never be reached in general.

$$\frac{1}{r}\frac{\partial}{\partial r}\left(r\frac{\partial p}{\partial r}\right) = \frac{0.000264k}{\varphi\mu c_t r_w^2}\frac{\partial p}{\partial t} \quad (34$$

$$p_w = p_{r_w} - \frac{kh}{141.2B_o\mu}S\left(r\frac{\partial p}{\partial r}\right)_{r=r_w} \quad (35$$

$$q_o = \frac{kh}{141.2B_o\mu}\left(r\frac{\partial p}{\partial r}\right)_{r=r_w} \quad (36$$

$$q_g = Rq_o \quad (37$$

$$q_w = \frac{fw}{1-fw}q_o \quad (38$$

Fluid properties. In order to compute fluid properties to be used in the model, general correlations are used throughout, although tabulated property values could also be considered in a more general case. It is important to note that fluid properties are required for a complete range of conditions ranging from high pressure and temperature associated with reservoir conditions to near atmospheric conditions encountered in the surface facilities. A variety of published correlations were considered, but most are confined to reservoir pressures and temperatures and lead to non-physical values when applied to surface conditions. For this reason the correlations of Vazquez and Beggs (1980) are used for black oil hydrocarbon systems, with several constraints necessary to avoid unreasonably low or negative compressibility. Water properties were represented with correlations documented in Whitson and Brulé (2000), while gas properties are computed from z-factors using Hall and Yarborough (1973) with viscosity from Lee et al. (1966). Since these are all standard correlations used widely in the industry, the details are not presented here, but can be found in Whitson (2000)

VALIDATION

To validate the model formulation, several tests were run. Figure 3 shows the predicted dynagraph for a 4000 ft well pumping 6 SPM with a 1.5 in pump in 2-7/8" anchored tubing as well as the predicted dynagraph using the QRod software (copyright Echometer, Inc.). It is apparent that the predicted dynagraphs are similar, but not identical. Since the model used in this work accounts for fluid momentum and variation in tubing pressure, a difference in the pump load can be observed as shown in Figure 4. Figure 5 also shows a wide variation in surface flow rate, including back flow (negative rate) due to fluid compressibility and momentum effects, even though the intake at the pump is always zero or positive.

Since most models do not handle complete transient flow and account for surface flowlines, it is difficult to find data showing the pressure variations. One set of data, however, was found (Pennebaker (2014)). It is known that the well was producing from about 2000 to 3000 ft with ¾" rods and 2-3/8" tubing into a 2" ID flowline. Unfortunately little other details of the well and facilities configuration are available, but an attempt was made to match the recorded tubing pressures. The raw data sampled at 10 Hz (100 msec between samples) are shown in Figure 6 where the pressure scale is relative to the analog-to-digital converter voltage units. The pressure peaks are estimated to be on the order of 150 psi and the lower pressure limit is about 50 psi. The well was operating at 12 SPM yielding 1 stroke every 5 sec. As can be seen there are 2 pressure peaks per cycle and although the cycles are very similar, they are not identical.

Figure 7 shows two simulations with a 3000 ft well with ¾" rods, 32" stroke, and 1-3/4" plunger in 2-3/8" tubing producing into a 2" ID flowline. The graph on the left shows a 2000 ft flowline, while the graph on the right shows a

1500 ft flowline. As can be seen, two pressure peaks are shown per cycle, with the shape varying somewhat due to the change in length of the flowline.

Also of interest is to view the corresponding tubing flow rate for the two cases, shown in Figure 8. As can be seen, one of the pressure peaks corresponds to a pulse of fluid being pumped from the well; however, the other peak corresponds to backflow from the flowline into the tubing caused by compressibility and momentum effects in the well and flowline.

OBSERVATIONS

Using the model it is possible to evaluate the effect of various assumptions normally used in rod pump models and also to suggest areas for further investigation in the development of surveillance efforts. As a result the model has currently been used to evaluate the effect of fluid viscosity and tubing diameter on the damping effect, the effect of interference between wells in a facility, and the potential for monitoring tubing pressures to determine impending artificial lift problems.

Effect of fluid and tubing on damping. Figure 9 shows the effect of oil gravity (mainly affecting fluid viscosity) on the predicted dynagraph, while Figure 10 shows the effect of tubing diameter. In all cases a 4000 ft well with ¾" rods and 1-1/2" pump plunger are operated at 6 SPM. As can be seen, the heavier (more viscous) oil yields a more rounded dynagraph indicative of more drag on the rods or a larger damping factor. In Figure 10 a 20 API oil was used for both tubing diameters. As can be seen, the larger tubing diameter appears to show a slightly lower damping due to reduced fluid velocity, but the difference is very small, since the plunger diameter is the same in both cases.

Interaction between wells in a facility. In order to show the effect of interference between wells through the surface facilities, a model with 2 wells operated at 5 and 6 SPM producing through flowlines of different length to a header, followed by a flowline to a constant pressure tank was implemented. A diagram of the model is shown in Figure 11, while pressures and flow rates at various points in the system are shown in Figures 12, 13, 14, and 15. Note that a cyclic behavior is observed at all points, but the cycles never quite repeat due to the complexity of the system. In essence the system seems to be approaching a somewhat chaotic state. The variation in tubing pressures caused by interaction between the wells can easily explain the variations shown in the measured data of Figure 6.

Use of tubing pressure for surveillance. In order to investigate the possibility of using wellhead (tubing) pressures for well surveillance purposes, a single well and flowline model was constructed as in the damping comparisons above. The well was 4000 ft deep, ¾" rods and a 1-1/2" plunger pumping 30 API oil at 6 SPM. The base case dynagraph and tubing pressure are shown in Figure 16 and the corresponding dynagraph and tubing pressure for the leaking traveling valve is shown in Figure 17. Although the dynagraphs appear close to identical, it is easy to note that the pressure peak indicated by the arrow in Figure 17 is reduced in the leaking traveling valve case. This difference indicates that it might be possible to use the tubing pressures to assist in diagnosing beam pumping problems, however, further work is needed to determine how to remove extraneous effects, such as inter-well interference through the flowlines.

CONCLUSIONS

Based on the integrated model documented in this paper, it is apparent that complex transient behavior should be expected in nearly all producing facilities. Especially with beam pumped wells, it is apparent that true steady state flow never occurs and when there are interactions between wells operating under different conditions, a nearly chaotic system of pressures and flow rates is to be expected.

Examples shown in this paper indicate that fluid viscous drag can be used to represent damping in the wave equation and the model developed here can be used to estimate the changes in damping factors expected due to variations in well geometry and fluid properties. Clearly, further work is needed to quantify these effects.

The integration of multiple wells with surface facilities indicates the complex behavior that can be observed, even with only two wells. Due to the complexity of the system, long term modeling of many wells with fully transient flow models is impractical, however, the current model can be used to evaluate assumptions and to define proxy models for more complex systems. In this respect the current model can serve as a research tool for further investigations into the complex system behavior herein identified.

The leaking traveling valve example shows that an effect on the tubing pressure should be observable, at least in some cases. Clearly the effect is minor and further work is needed to determine how to separate the pressure signal due to the leaking valve from other effects in the pressure data. With the possibility of near chaotic behavior due to interference between multiple wells, it is apparent that additional work is needed.

Finally, in view of the variety of transient responses noted in modeling various simplified facilities, it is apparent that much work remains to be done to identify methods useful for surveillance of artificial lift systems and facilities. In addition, the effect of reservoir flow, completion skin, and related effects have not yet been evaluated. As a result it seems that a more complete evaluation of these effects is an open field for further investigations.

Since the measurement of surface pressures is relatively simple, even at sample rates of several tens of Hertz, it seems that the development of surveillance methods based on such measurements can be quite useful in the operation of marginal wells, many of which are produced by beam pump.

NOMENCLATURE

α	Acoustic velocity in rod material (ft/sec)
a_a	Surface pumping unit parameter
A_r	Rod cross sectional area (ft^2)
B_o	Oil formation volume factor (bbl/ST bbl)
c_t	Total rock and fluid compressibility (1/psi)
C	API surface pumping unit parameter
C_1, C_2, C_3, C_4	Parameters used in surface pumping unit model
D_c	Rod coupling diameter (ft)
D_r	Rod diameter (ft)
D_t	Tubing diameter (ft)
E_r	Young's modulus or rod material (psi)
f_w	Water cut, volume fraction of water in liquid (fraction)
f^n_{Gi}	Gas momentum balance for segment i, time step n
f^n_{Li}	Liquid momentum balance for segment i, time step n
F_{aG}	Drag force on gas due to pipe annulus (lbf/ft)
F_{aL}	Drag force on liquid due to pipe annulus (lbf/ft)
F_{wL}	Drag force on liquid due to pipe wall (lbf/ft)
F_{GL}	Drag force on liquid due to gas interface (lbf/ft)
F_{wL}	Drag force on liquid due to pipe wall (lbf/ft)
g, g_c	Gravitation constant (32.17 ft/sec^2)
g^n_{Li}	Liquid mass balance for segment i, time step n
g^n_{oi}	Oil mass balance for segment i, time step n
g^n_{Ti}	Total mass balance for segment i, time step n
h_G	Gas enthalpy (BTU)
h_G	Liquid enthalpy (BTU)
G, H	API surface pumping unit parameters
H_G	Gas holdup, volume fraction of gas (fraction)
H_L	Liquid holdup, volume fraction of liquid (fraction)

H	Reservoir thickness (ft)
h^n_{Ti}	Total energy balance for segment i, time step n
I	API surface pumping unit parameter
J_c	Mechanical equivalent of heat (778.17 ft-lbf/BTU)
K	Permeability (md)
L_2	Parameter used in surface pumping unit model
p	Pressure (psia)
p_r	Reservoir pressure at radius r (psia)
p_w	Wellbore bottomhole pressure (psia)
P	API surface pumping unit parameter
q_g	Gas volumetric flow rate (MSCF/day)
q_o	Oil volumetric flow rate (ST bbl/day)
q_w	Water volumetric flow rate (ST bbl/day)
r	Reservoir radius (ft)
r_w	Wellbore radius (ft)
R	Gas-oil ratio (MSCF/ST bbl)
R	API surface pumping unit parameter
R_{eG}	Gas Reynolds number (dimensionless)
R_{eL}	Liquid Reynolds number (dimensionless)
S	Perimeter (ft)
S	Wellbore damage skin factor (dimensionless)
SPM	Strokes per minute of surface pumping unit
t	Time (sec)
T	Temperature (F)
T_{ext}	External temperature (F)
u	Displacement of rod (ft)
U	Heat loss coefficient (BTU/sec/F/ft^2)
v_G	Gas velocity (ft/sec)
v_L	Liquid velocity (ft/sec)
V_g	Standard volume of gas in pump barrel (MSCF)
V_o	Standard volume of oil in pump barrel (ST bbl)
V_w	Standard volume of water in pump barrel (ST bbl)
V_p	Internal pump volume (ft^3)
x	Distance (ft)
α, β	Parameters used in surface pumping unit model
ϕ	Porosity (fraction)
μ	Reservoir fluid viscosity (cp)
μ_G	Gas phase viscosity (cp)
μ_L	Liquid phase viscosity (cp)
ρ_G	Gas phase density (lbm/ft^3)
ρ_L	Liquid phase density (lbm/ft^3)
ρ_o	Oil density (lbm/ft^3)
ρ_r	Density of rod material (lbm/ft^3)
θ	Angle of pipe or pumping unit (radians)
θ_c	Angle of pumping unit crank at rest (radians)

REFERENCES

Aho, A.V., Hopcroft, J.E. and Ullman, J.D.1983 *Data Structures and Algorithms*, Addison-Wesley Publishing Company.

De Almeida Barreto Filho, M.2001 'Estimation of Average Reservoir Pressure and Completion Skin Factor of Wells that Produce Using Sucker Rod Pumping', University of Texas at Austin

Daugherty, R.L. and Franzini, J.B.1965 *Fluid mechanics with engineering applications*, . New York: McGraw-Hill.

Earlougher, R.C.1977 'Monograph vol. 5: Advances in Well Test Analysis', *Soc. Pet. Eng.* 90–104

Everitt, T.A. and Jennings, J.W.1992 'An improved finite-difference calculation of downhole dynamometer cards for sucker-rod pumps', *SPE Prod. Eng.* 7, 121–27

Gibbs, S.G.1963 'Predicting the Behavior of Sucker-Rod Pumping Systems', *J. Pet. Technol.* 15,

Govier, G.W. and Aziz, K.2008 *The Flow of Complex Mixtures in Pipes*, (2nd Edition,). Richardson, TX: Society of Petroleum Engineers.

Gray, H.E.1963 'Kinematics of Oil-Well Pumping Units', *Drill. Prod. Pract.*

Hall, K.R. and Yarborough, L.1973 'A new equation of state for Z-factor calculations', *Oil Gas J.* 71, 82–92

Himmelblau, D.M. and Bischoff, K.B.1968 *PROCESS ANALYSIS and SIMULATION: Deterministic Systems*, . New York, NY: John Wiley & Sons, Inc.

Lee, A., González, M. and Eakin, B.1966 'The viscosity of natural gases', *J. Pet. Technol.* 18, 997–1000

Lekia, S.D.L. and Evans, R.D.1995 'A Coupled Rod and Fluid Dynamic Model for Predicting the Behavior of Sucker-Rod Pumping Systems. Part 1: Model Theory and Solution Methodology', *SPE Prod. Facil. Soc. Pet. Eng. U. S.* 10:1,

Pennebaker, S.2014. 'Personal Communication'

RELAP52012 *RELAP5-3D© Code Manual Volume I: Code Structure, System Models and Solution Methods*, Idaho National Laboratory.

Shirdel, M.2010 'Development of a Coupled Wellbore-Reservoir Compositional Simulator for Horizontal Wells', MS Thesis, University of Texas

Shoham, O.2006 *Mechanistic Modeling of Gas-Liquid Two-Phase Flow in Pipes*, . Richardson, TX: Society of Petroleum Engineers.

Valeev., M.D. and Repin, N.N.1976 'IZVESTIYA VYSSHIKH VCHEBNYKH ZAVEDENII', *NEFT GAZ* 8, 33–44

Vazquez, M. and Beggs, H.D.1980 'Correlations for fluid physical property prediction', *J. Pet. Technol.* 32, 968–70

Whitson, C.H. and Brulé, M.R.2000 *Phase Behavior*, Vol 20 Richardson, TX: Monograph Series, SPE.

ACKNOWLEDGEMENTS

Special thanks to Dr. Patzek and Dr. Sepehrnoori for advice in the implementation of the field model, to Dr. Mahdy Shirdel for many discussions on multiphase flow model and assorted complexities, and to Strode Pennebaker for discussions and data used to confirm the model predictions.

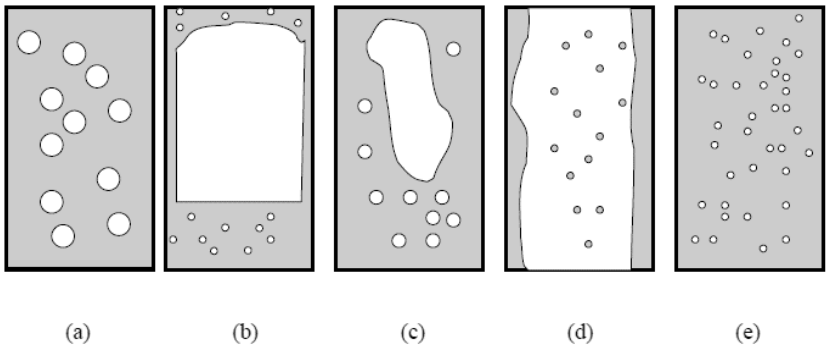

Figure 1 - Schematic view of vertical flow regimes, a) bubbly flow, b) slug flow, c) churn flow, d) annular flow, e) disperse bubble flow (From Shirdel, 2010)

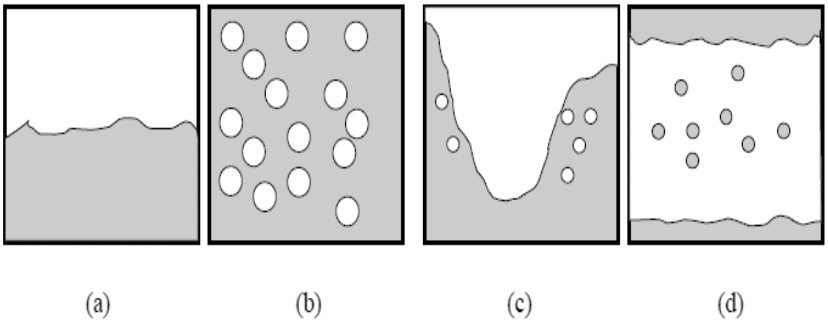

Figure 2 - Schematic view of vertical flow regimes, a) stratified flow, b) bubbly flow, c) intermittent flow, d) annular flow (From Shirdel, 2010)

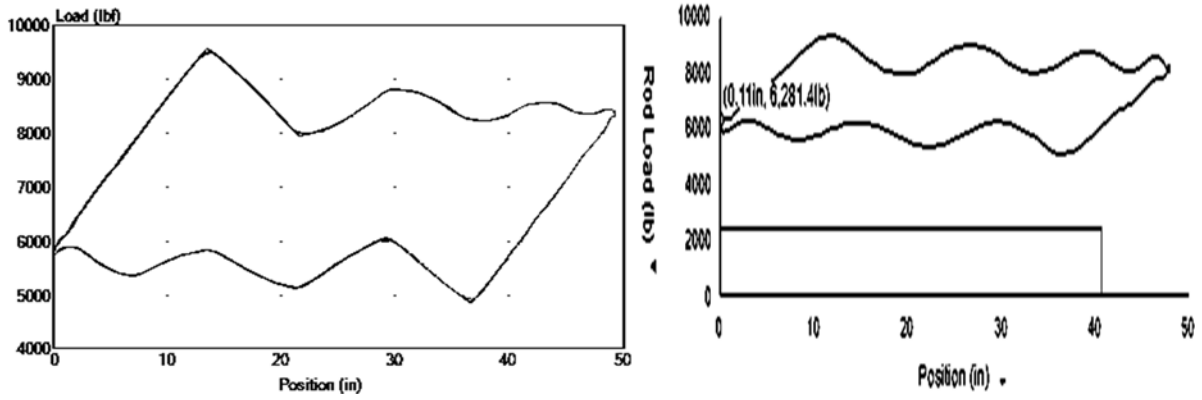

Figure 3 - Comparison of Predicted Dynagraphs, 4000 ft, 6 SPM, 1.5” plunger. ¾” rods in 2-7/8” tubing

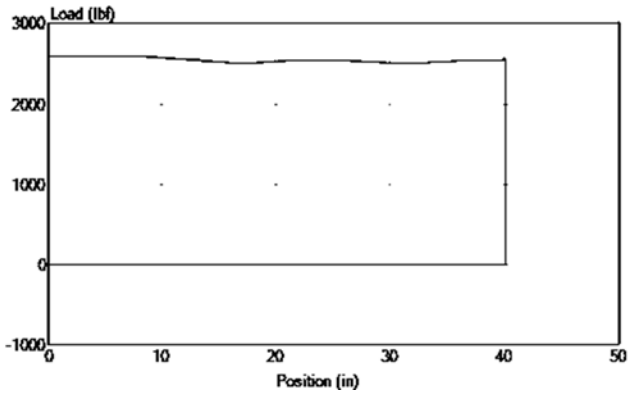

Figure 4 - Computed Pump Dynagraph, 4000 ft, 6 SPM, 1.5” plunger. ¾” rods in 2-7/8” tubing

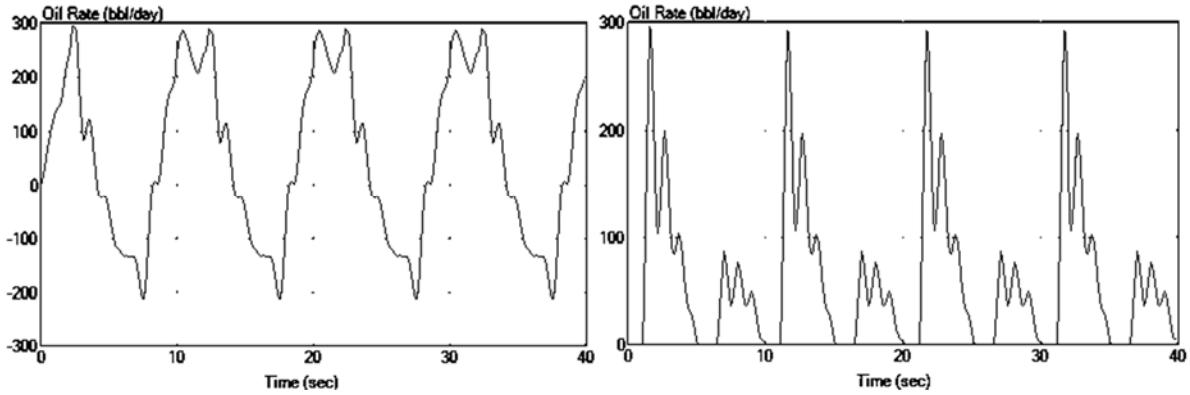

Figure 5 - Computed Surface and Pump Oil Rate, 4000 ft, 6 SPM, 1.5” plunger. ¾” rods in 2-7/8” tubing

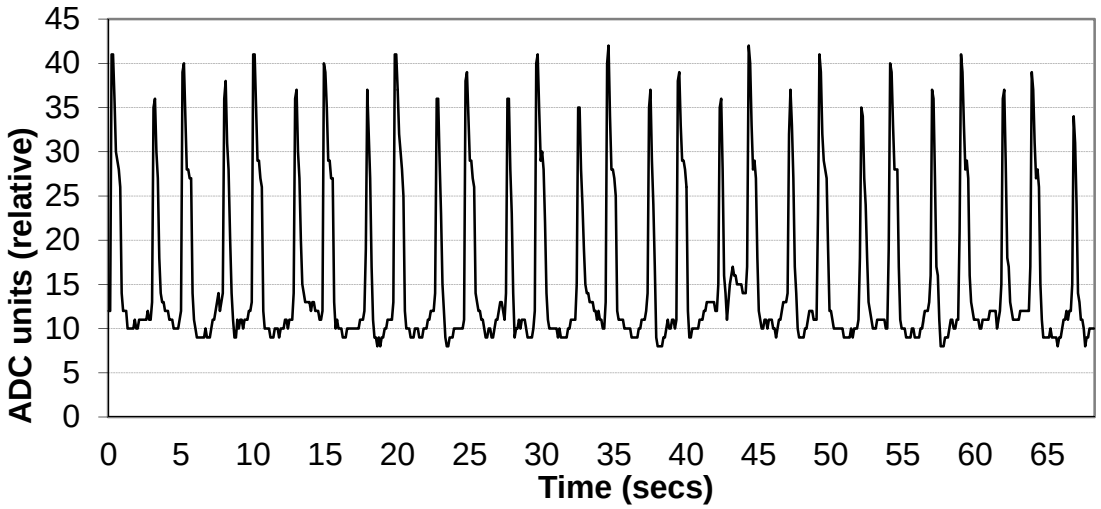

Figure 6 - Measured Flowline Pressures in Beam Pumping Well

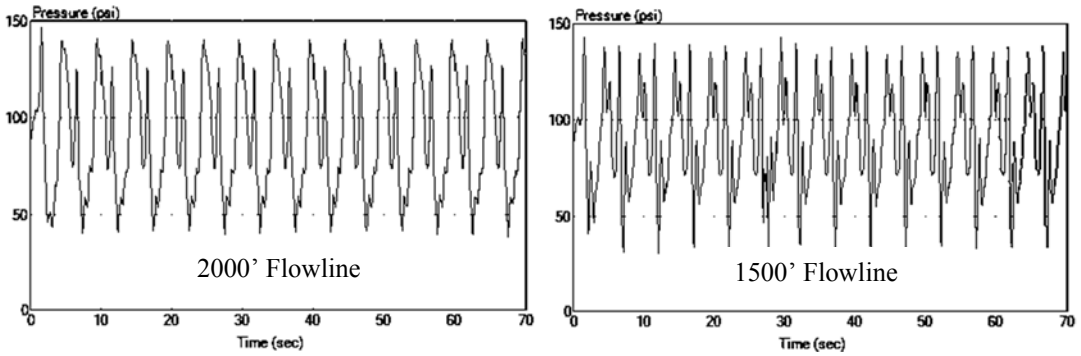

Figure 7 - Predicted Flowline Pressures in Beam Pumping Well with 2000' and 1500' Flowline

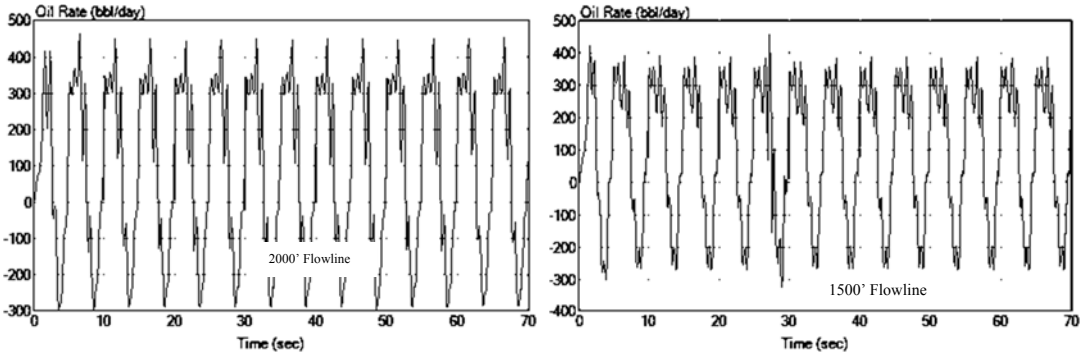

Figure 8 - Predicted Flowline Pressures in Beam Pumping Well with 2000' and 1500' Flowline

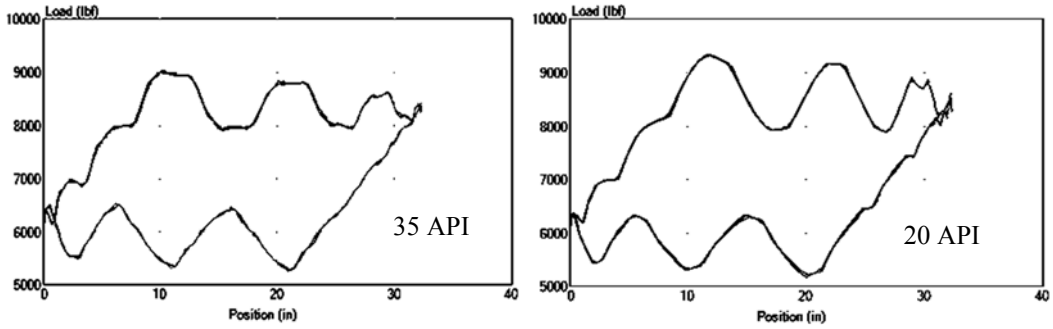

Figure 9 - Predicted Dynagraph for 4000' well. Effect of viscosity

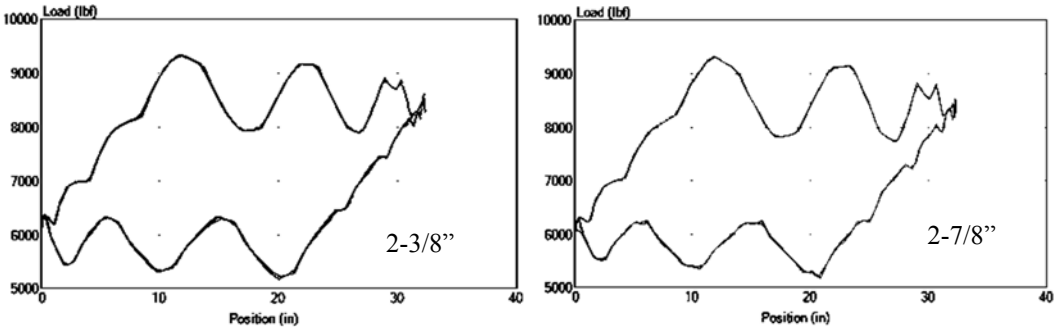

Figure 10 - Predicted Dynagraph for 4000' well. Effect of tubing size

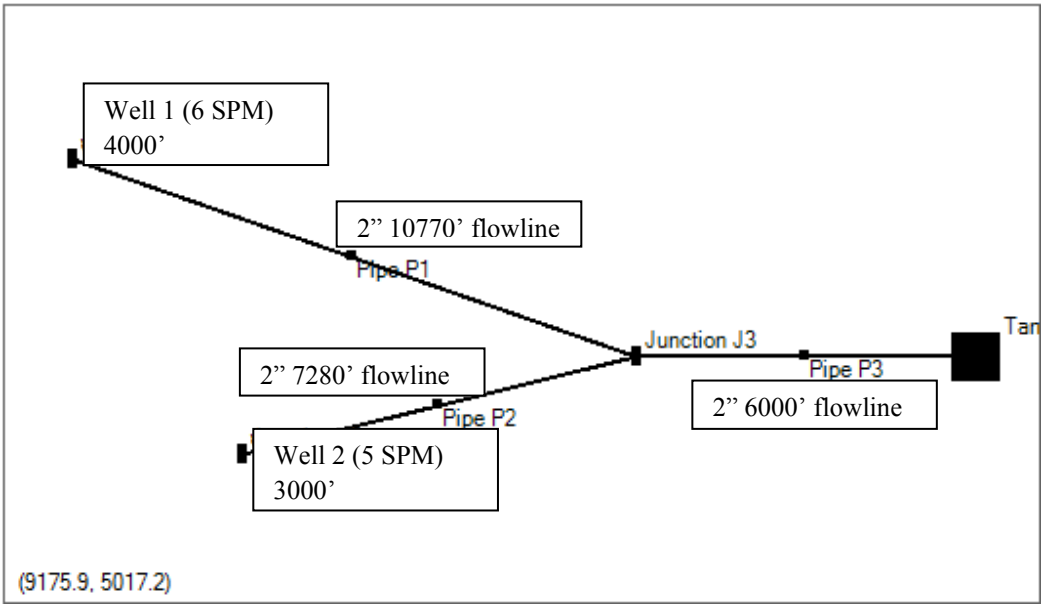

Figure 11 - Diagram of Two Well Facility

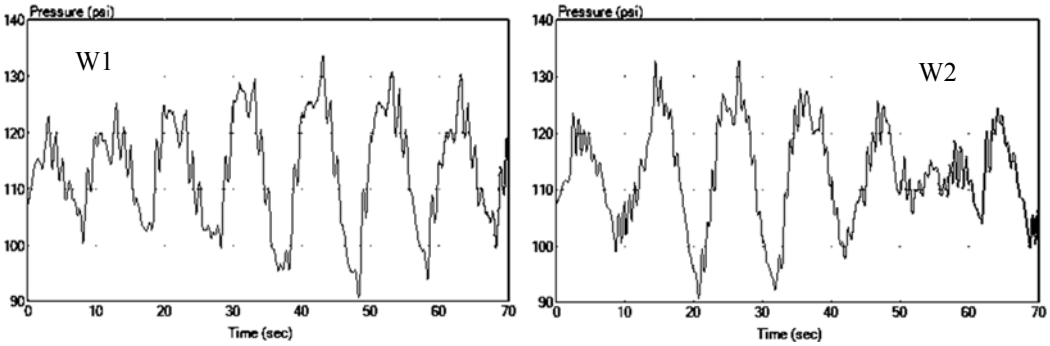

Figure 12 - Tubing pressure of wells in 2 well facility

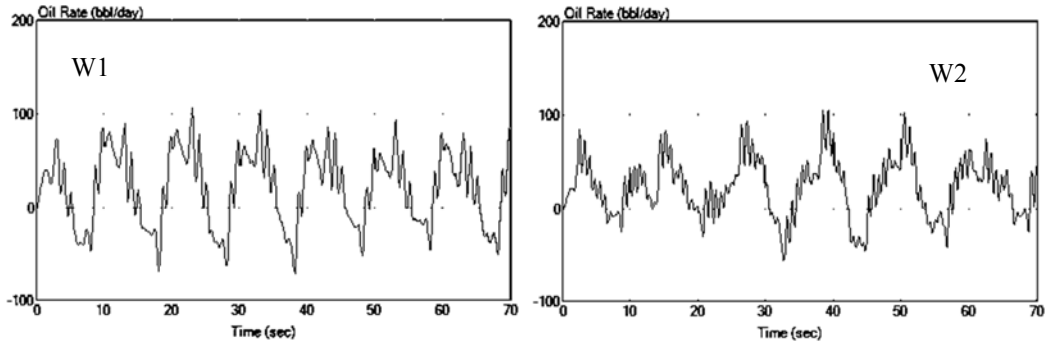

Figure 13 - Wellhead rate of wells in 2 well facility

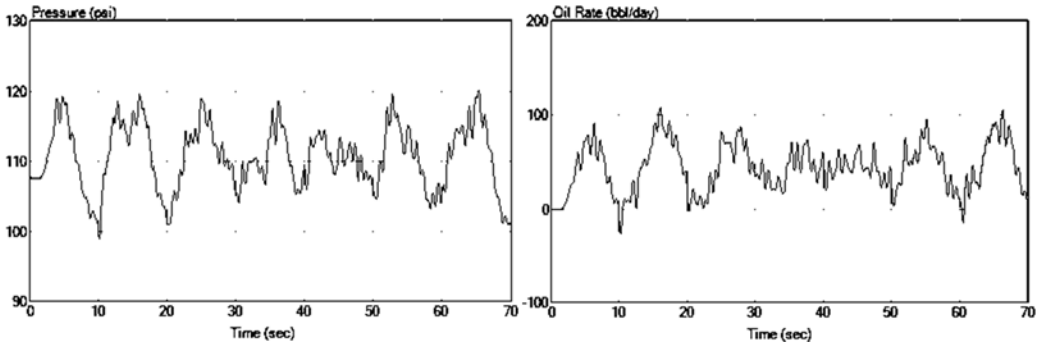

Figure 14 - Header pressure and rate in 2 well facility

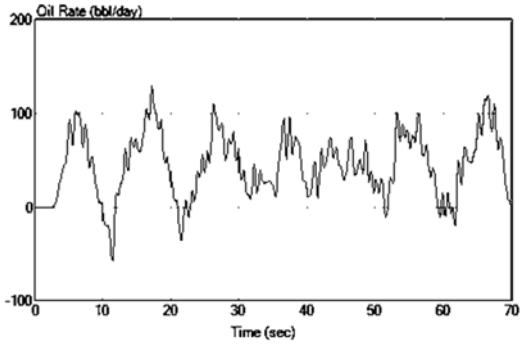

Figure 15 - Outlet rate in 2 well facility

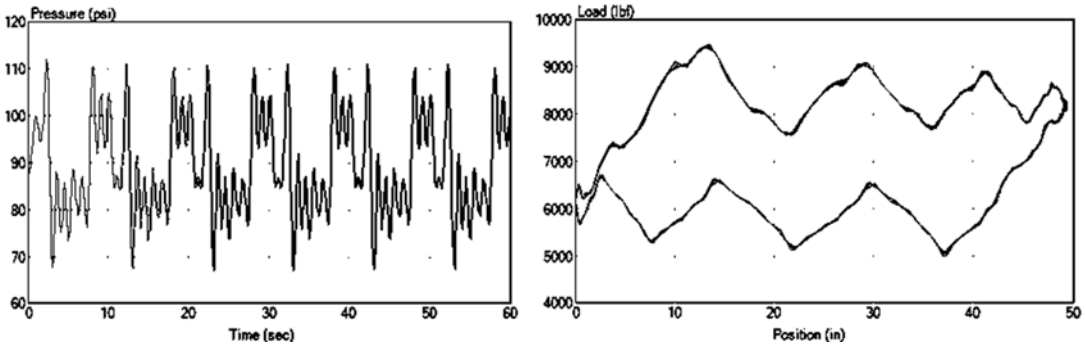

Figure 16 -Tubing pressure and dynagraph, normal traveling valve

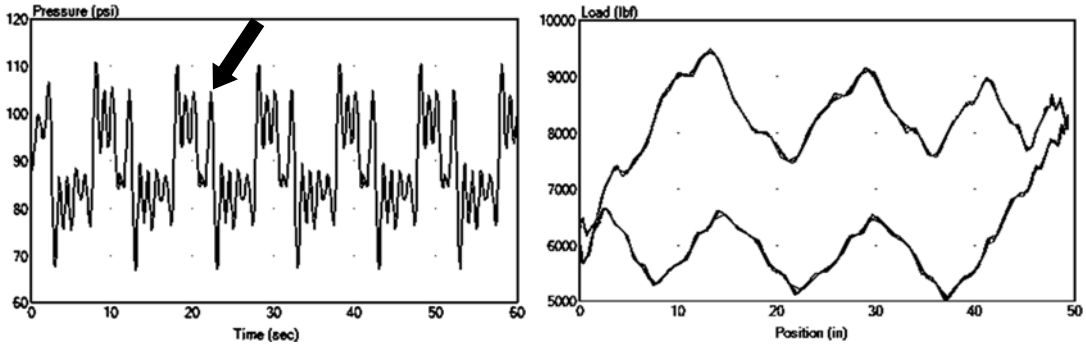

Figure 17 - Tubing pressure and dynagraph, leaking traveling valve